JOURNAL OF THE ROYAL SOCIETY Interface

J. R. Soc. Interface (2012) **9**, 313–327
doi:10.1098/rsif.2011.0278
Published online 29 June 2011

Surface wettability of plasma SiO_x:H nanocoating-induced endothelial cells' migration and the associated FAK-Rho GTPases signalling pathways

Yang Shen[1,2], Guixue Wang[2], Xianliang Huang[1], Qin Zhang[2], Jiang Wu[1], Chaojun Tang[2], Qingsong Yu[3] and Xiaoheng Liu[1,*]

[1]*Institute of Biomedical Engineering, School of Preclinical and Forensic Medicine, Sichuan University, Chengdu 610041, People's Republic of China*
[2]*Key Laboratory of Biorheological Science and Technology (Chongqing University), Ministry of Education, Bioengineering College of Chongqing University, Chongqing 400030, People's Republic of China*
[3]*Center for Surface Science and Plasma Technology, Department of Mechanical and Aerospace Engineering, University of Missouri, Columbia, MO 65211, USA*

Vascular endothelial cell (EC) adhesion and migration are essential processes in re-endothelialization of implanted biomaterials. There is no clear relationship and mechanism between EC adhesion and migration behaviour on surfaces with varying wettabilities. As model substrates, plasma SiO_x:H nanocoatings with well-controlled surface wettability (with water contact angles in the range of $98.5 \pm 2.3^\circ$ to $26.3 \pm 4.0^\circ$) were used in this study to investigate the effects of surface wettability on cell adhesion/migration and associated protein expressions in FAK-Rho GTPases signalling pathways. It was found that EC adhesion/migration showed opposite behaviour on the hydrophilic and hydrophobic surfaces (i.e. hydrophobic surfaces promoted EC migration but were anti-adhesions). The number of adherent ECs showed a maximum on hydrophilic surfaces, while cells adhered to hydrophobic surfaces exhibited a tendency for cell migration. The focal adhesion kinase (FAK) inhibitor targeting the Y-397 site of FAK could significantly inhibit cell adhesion/migration, suggesting that EC adhesion and migration on surfaces with different wettabilities involve (*p*)FAK and its downstream signalling pathways. Western blot results suggested that the FAK-Rho GTPases signalling pathways were correlative to EC migration on hydrophobic plasma SiO_x:H surfaces, but uncertain to hydrophilic surfaces. This work demonstrated that surface wettability could induce cellular behaviours that were associated with different cellular signalling events.

Keywords: plasma SiO_x:H nanocoating; surface wettability; cell adhesion/migration; FAK-Rho GTPases signalling pathways

1. INTRODUCTION

There is increasing evidence that vascular endothelial cell (EC) adhesion and migration are essential processes in angiogenesis, wound healing, vessel remodelling and re-endothelialization [1]. In particular, regarding implanted biomaterials such as coronary stents, research has indicated that in-stent restenosis could be decreased by rapid surface endothelialization of a cardiovascular stent, which was regarded as an important means to prevent thrombogenicity, to reduce proliferation and migration of smooth muscle cells (SMCs) [2]. Neighbouring migration of vascular ECs on a stent surface is the main process of re-endothelialization after stent implantation. The results of early experimental works suggested that the sequence of healing events after intravascular stent placement, marked by SMCs' migration and proliferation and extracellular matrix (ECM) accumulation, ceased after complete coverage of ECs. The rate of EC coverage is influenced more by migration than by proliferation [3]. However, other evidence indicated that endothelial progenitor cells from circulatory blood contributed to vascular repair and stent re-endothelialization [4,5]. Regardless of cell source in stent endothelium, from blood circulation or vessel wall, it is important to properly modify the implanted surface with suitable surface properties for EC adhesion and migration.

Non-stoichiometric silicon oxides (SiO_x with $0 < x \leq 2$) have been widely applied as optical coatings, passivation layers and interlayers in electronics owing to their low dielectric constant (low-*k*) [6,7]. SiO_x:H coatings prepared

*Author for correspondence (liuxiaohg@sina.com).

Electronic supplementary material is available at http://dx.doi.org/10.1098/rsif.2011.0278 or via http://rsif.royalsocietypublishing.org.

Received 4 May 2011
Accepted 10 June 2011

by low-temperature plasma deposition may have well-controlled surface wettability via mediating plasma gas compositions, e.g. using trimethysilane (TMS; $(CH_3)_3SiH$) and O_2 with different molar ratios. In addition, in our recent studies, low-temperature plasma-coated nitinol alloy with hydrophilic SiO_x:H nanocoatings showed excellent biocompatibility and cell affinity [8,9]. To our knowledge, there are very few studies focusing on implanted materials coated with plasma SiO_x:H nanocoatings. One example is the surface functionalization of amorphous hydrogenated silicon (a-Si:H) and amorphous silicon suboxide films (a-SiO_x:H) with Arg-Gly-Asp (RGD)-peptides by hydrosilylation reactions [10].

Cell adhesion and migration are affected by chemical composition, mechanical properties, wettability and roughness of the substrates [11]. In turn, surface wettability is determined by surface chemistry and roughness. On the other hand, surface wettability determines protein and cell adhesion behaviour [12,13]. However, the effects of surface wettability on cell migration are not clear. In a manner similar to chemical and mechanical stimulus, the properties of materials, especially surface information, are important factors to determine cells' biological behaviour, which induce a cascade of intercellular signalling events. The different surface properties would induce different ECM protein adsorption, such as fibronectin (FN), laminin (LN) and vitronectin (VN) [14,15], which are ligands of integrins on cell membrane. The integrins $\alpha2\beta1$ and $\alpha5\beta1$ were primarily thought of as LN and FN receptors, respectively, while $\alpha3\beta1$ has been shown to be capable of binding to multiple ligands including both FN and LN [16]. The distribution of active integrins would result in focal adhesion conformation, which induces phosphorylation of focal adhesion kinase (FAK) at initial tyrosine-397 site. The interaction between the Y397-activated FAK leads to a cascade of tyrosine phosphorylation of multiple sites in FAK (Y-576, -577, -925) and activation of other downstream signalling pathways. FAK can influence the activity of Rho-family GTPases (RhoA, Rac and Cdc42) through a direct interaction with, or phosphorylation of protein activators or inhibitors of Rho GTPases, which could result in direct local actin assembly to form stress fibres, lamellipodia or filopodia [17]. Rac1 is one of the small G proteins, which plays a vital role in cell migration behaviour. The current studies have shown that Rac1 is required in the front of the migrating cell to regulate actin polymerization and lamellipodia and to form membrane protrusion [18].

Accordingly, we hypothesized that cell adhesion and migration on surfaces with varying wettabilities induce FAK-Rho GTPases signalling events. The phosphorylation of FAK could regulate Rac1 protein expression and mediate cell migration behaviour. In this study, an *in vitro* investigation on cell adhesion/migration was firstly performed with a hydrophobic–hydrophilic SiO_x:H coating, and the relative protein expression in FAK-Rho GTPases signalling pathway was examined.

2. MATERIAL AND METHODS

In this study, polished silicon (100) wafers (150 mm in diameter, 6.082–12.55 Ωcm in resistivity, *p*-type with boron as a dopant, Silicon Valley Microelectronics, Inc., Santa Clara, CA, USA) with very smooth surfaces were used to explore treatment conditions of plasma coating. The plasma-coated wafers were used to examine *in vitro* cell adhesion and migration. A human vascular EC line, EA.hy926 (Hematology Research Institute of Jiangsu Province, China), was used in this study; this is a hybridoma cell line between human umbilical vein ECs (HUVECs) and the epithelioma A549 cells, and retains most of the features of the HUVECs, including the expression of endothelial adhesion molecules and human factor VIII-related antigen [19].

2.1. Plasma coating and surface characterization

A low-temperature plasma deposition technique was used to prepare SiO_x:H nanocoating on the smooth surface of the silicon wafers, which were performed at the Centre for Surface Science and Plasma Technology in University of Missouri (Columbia, MO, USA). A bell jar-type plasma reactor system was used in this study, which was described previously in our recent research [20]. Before plasma deposition, the wafers were pre-treated and cleaned with oxygen plasma for 2 min under conditions of 2 sccm oxygen flow, 25 mtorr pressure and 5 W DC power input. Subsequently, plasma SiO_x:H nanocoatings with thickness controlled at 30–40 nm were deposited in a mixture of TMS and oxygen (from 0 to 5 sccm) under conditions of 25 mtorr and 5 W of DC power input. The sample identification codes and preparation conditions used in this study are summarized in table 1.

2.2. Surface properties analyses

After plasma coating of silicon wafers, the coating thickness was detected by a null seeking type AutoEL-II Automatic Ellipsometer (Rudolph Research Corporation, Flanders, NJ, USA) with a 632.8 nm helium–neon laser light source. The surface wettability of plasma-coated films was assessed by using a contact angle measurement system (VCA 2500XE, USA). X-ray photoelectron spectroscopy (XPS; Escalab 250, Thermo, USA) with a monochromatic AlKα X-ray source was used to determine the composition and chemical states of the plasma coating (500 μm scanning range). Adhesion strength of each plasma SiO_x:H nanocoating on the silicon wafers was evaluated using a WS-2005 scratch test apparatus (Chemistry and Physics Institute, Lanzhou, China).

2.3. In vitro *cell adhesion assay*

The plasma-coated silicon wafers (three specimens for each treatment condition) were cut into a $1 \times 1\ cm^2$ square, and then were put into a six-well polystyrene tissue culture plate. UV light was then used to sterilize the specimens for at least 2 h. EA.hy926 cells were dissociated mechanically and enzymatically in flasks with 0.25 per cent trypsin, and then suspended in 10 per cent serum-containing media. Cell density at 1.0×10^3 cells ml^{-1} was regulated by haemocytometer and added into six-well polystyrene tissue culture plates co-cultured with plasma-coated silicon wafers.

Table 1. Sample identification codes and preparation conditions.

identification codes of samples	flow radio of TMS and O_2 (sccm)	deposition duration (min)
1:0	TMS:O_2 = 1:0	1.5
1:1	TMS:O_2 = 1:1	2
1:2	TMS:O_2 = 1:2	3
1:3	TMS:O_2 = 1:3	5
1:4	TMS:O_2 = 1:4	6
1:5	TMS:O_2 = 1:5	7

After 4 and 8 h, the number of initial cells adhered to each specimen was examined by microscopy (UM203i, UOP Company, China). Three specimens for each treatment condition, and five representative areas on each specimen, were randomly chosen for taking pictures. According to the pictures, different cell behaviours including suspension, just adhesion (but not spreading) and spreading were distinguished and counted. Summing up total cell numbers in the five representative areas, the average number of cells on each treatment condition was calculated and presented as mean $\pm$ s.d.

After 1 and 5 days, the F-actin distribution (stained by Phallotoxins, Invitrogen, USA) and morphologies of adhered cells on each specimen were examined using a laser scanning confocal microscope (Leica TCS SP5, Germany) and a scanning electron microscope (Quanta 600F, FEI Company, USA), respectively.

2.4. Cells' migration on plasma SiO_x:H coating—scratch wound migration assay

Cell migration was measured using a monolayer scratch injury assay as described previously [21]. Briefly, the EA.hy926 cells were plated onto plasma SiO_x:H-coated silicon wafers until confluence and then starved serum-free for 8 h. During the last 4 h, hydroxyurea was added at a final concentration of 5 mmol l^{-1} to prevent further DNA synthesis. Then a uniform scratch (about 500 μm) was performed in the cell monolayer using a plastic cell scrapper (Corning, USA). Then, cell monolayers were washed gently with phosphate-buffered saline (PBS), marked (for reference) and photographed using a reflective upright biological microscope (UM203i). Images of the wounds under static culture in an incubator containing 5 per cent CO_2 at 37°C without serum were acquired at 0, 2, 6 and 12 h. Eight wounded edges in the cross section were randomly chosen at 0 h and observed consecutively at each duration. The cell migration distance at the end of each recording period was calculated by difference between the end length and original length of the wounded edge. Migrated cell numbers were derived from the average of the fields in triplicates. After 12 h, by continuing culturing, and by observing per half-hour periods until cells reached confluency again, wound repair durations of each sample were determined.

2.5. Single cells' motility on surfaces with different wettabilities

After 4 h culture, single cells spreading on plasma-coated samples were randomly chosen for observation. With a fixed view and focus, images at 0, 10, 20 and 30 min were taken, and the migrated distances of single cells were calculated by $D_n = L_n - L_0$, where D_n is the cell migration distance, L_n and L_0 are the cell position at the ending point and at the original position, respectively. Accordingly, during 30 min, the average migrated speed of cells of each group was calculated.

2.6. FAK inhibitor

FAK inhibitor (1, 2, 4, 5-benzenetetraamine tetrahydrochloride), targeting the Y-397 site of FAK (Sigma, USA), increases cell detachment and inhibits cell adhesion in a dose-dependent manner, which was found and tested by Golibovskaya in 2008 [22]. In this study, it was used to explore whether the (p)FAK signalling pathway is important in inducing EC migration on the plasma SiO_x:H surface.

At first, scratch wound migration assays as described above were performed to determine the appropriate concentrations of the FAK inhibitor. Different concentrations of the FAK inhibitor (50, 100, 150, 200 and 250 nmol ml^{-1}) were added into 6-well tissue culture polystyrene (TCPS) plates co-cultured with cell scratch monolayer. Images of the wounds were acquired and analysed at 0, 2, 4, 8 and 24 h. According to the results, one certain concentration of the FAK inhibitor would be chosen to add into the sterilized plasma SiO_x:H-coated substrate. The same steps described in §§2.4 and 2.5 were repeated to investigate whether cell migration on surfaces with varying wettabilities would associate with the FAK Y-397 phosphorylation.

2.7. Western blot and immunofluorescence analyses—proteins associated with FAK signalling pathways

EA.hy926 cells were seeded at 1000 cells mm^{-2} for 24 h on SiO_x:H plasma-coated wafers. After 48 h culture, cells on each wafer with 70–80% confluence were washed three times with PBS and disintegrated by 50 μl cell lysis solution. The total proteins were collected and centrifuged with 10 000 r.p.m. at 4°C for 5–10 min. The protein concentration of each sample was quantified by UV spectrophotometer (DU 800, Beckman Coulter, Inc., CA, USA) using bicinchoninic acid protein assay kit. Equal amounts (30 μg) of total protein were added and separated by 10–12% sodium dodecylsulphate–polyacrylamide gel electrophoresis and blotted onto polyvinylidene fluoride (PVDF, GE Healthcare) transfer membranes. PVDF membranes were blocked for 2 h with 5 per cent bovine serum albumin (BSA) in TBST buffer (20 mmol l^{-1} Tris–HCl (pH 8.0), 150 mmol l^{-1} NaCl, 0.05% Tween 20). Membranes were incubated with the primary antibodies in 5 per cent BSA in TBST buffer overnight at 4°C. Following incubation with primary antibody, blots were washed three times with TBST buffer and incubated with appropriate horseradish peroxidase-labelled secondary antibodies in 1 per cent BSA in TBST buffer for 2 h at 37°C. After blots were washed with Tris-buffered saline Tween-20 (TBST), target proteins were detected using enhanced chemiluminescence. Images of bands were determined using

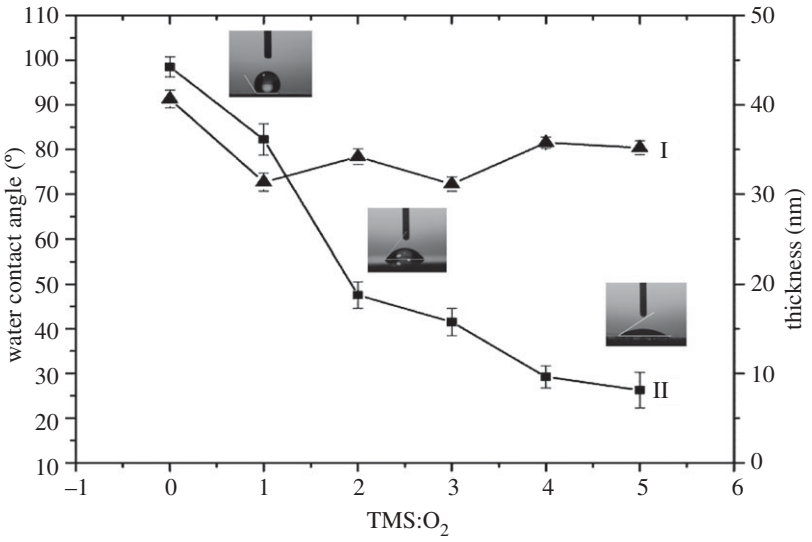

Figure 1. Oxygen flow rate dependence of the water surface contact angles (denoted as II) and thickness (denoted as I) of SiO_x:H plasma nanocoatings. Other plasma conditions used were: TMS flow rate of 1 sccm, system pressure of 25 mtorr, DC plasma power of 5 W.

Molecular Image ChemiDoc XRS$^+$ with Image Lab Software (Bio-Rad Laboratories, Inc., USA). All first antibodies, including anti-integrin α2 (C-9) mouse mAb (sc-74466), anti-integrin α5 (A-11) mouse mAb (sc-166665), anti-FAK (A-17) rabbit mAb (sc-1688), anti-*p*FAK (2D11) mouse mAb (against a phosphopeptide corresponding to amino acid residues surrounding tyrosine 397 of FAK of human origin, sc-81493), anti-Rac1 (C-11) rabbit mAb (sc-59) and anti-RhoA (26C4) mouse mAb (sc-418), were purchased from Santa Cruz Biotechnology, Inc. (CA, USA). The peroxidase-conjugated goat anti-mouse IgG and goat anti-rabbit IgG (secondary antibodies) were purchased from Dingguo Biotechnology Co., Ltd. (Beijing, China).

After 48 h in culture (equal to culture duration of Western blot analysis), immunofluorescence staining of RhoA and Rac1 was analysed by laser scanning confocal microscope (Leica TCS SP5). Cells were fixed with 4 per cent paraformaldehyde (Sigma-Aldrich) and permeabilized with 1 per cent Triton X-100 for 10 min. Following fixation and permeabilization, samples were blocked by adding 1 per cent (w/v) BSA for 15 min at room temperature. Cells were incubated in the primary anti-Rho and anti-Rac1 antibody solutions (1:100 dilution, Santa Cruz, USA) at 4°C overnight. Each step was followed by washing three times with PBS for 5 min every time. The secondary fluoresceine isothiocyanate (FITC)-conjugated immunoglobulin (goat anti-mouse IgG, green colour fluorescence) and PE-conjugated immunoglobulin (goat anti-rabbit IgG, red colour fluorescence) were incubated with primary anti-Rho and anti-Rac1 antibodies, respectively, for 60 min. Then, the DAPI (4′,6′-diamidino-2-phenylindole) with 1:800 dilution was added for nuclei staining for 30 min. Samples were sealed using 10 per cent glycerol, kept in a dark place and observed by laser scanning confocal microscopy.

2.8. Statistical analyses

The data obtained in this study were analysed using statistical software SPSS v. 11.5 (SPSS, Inc., Chicago, IL, USA) and reported as means $\pm$ s.d. Data obtained from different treatment groups were then statistically compared. To reveal differences among the groups, one-way ANOVA followed by Tukey's test was used. The differences were considered significant at $p < 0.05$.

3. RESULTS

3.1. Coating thickness and surface contact angles

Figure 1 shows oxygen flow rate dependence of the water contact angle and thickness of SiO_x:H plasma nanocoatings. It can be seen that, with the increase of oxygen ratio, the water contact angle of the samples decreased from $98.5 \pm 2.3^\circ$ to $26.3 \pm 4.0^\circ$ (the contact angle of silicon wafer without SiO_x:H plasma nanocoatings is about 55°, and not used in this study as control). A contact angle of 65° is regarded as the boundary between hydrophilicity and hydrophobicity [23]. In this study, 1:0 and 1:1 (TMS:O_2 ratio; table 1) groups showed hydrophobic properties, with contact angles of $98.5 \pm 2.3^\circ$ and $82.3 \pm 3.5^\circ$, respectively. Groups 1:2 and 1:3 showed neutral hydrophilicity with contact angles of $47.5 \pm 3.0^\circ$ and $41.5 \pm 3.0^\circ$, respectively, while 1:4 and 1:5 groups showed hydrophilicity with contact angles of $29.3 \pm 2.5^\circ$ and $26.3 \pm 4.0^\circ$, respectively. The thickness of all samples was controlled at 30–40 nm by adjusting the duration of plasma deposition.

The adhesion forces measured by WS-2005 scratch test instrument were used to evaluate the adhesion of plasma SiO_x:H coating to the silicon wafer substrate. During the measurements, an increasing force via the moving diamond indenter with a diameter of 0.2 mm was loaded on the surface of the plasma-coated samples. Acoustic signals were then captured by the piezoelectric transducer and the typical measurement data are shown in figure 2. Usually, the appearance of a second symmetrical peak can be regarded as breaking of the coating and the breaking point gives the critical loading. Plasma-coated samples deposited with TMS:O_2 ratios of

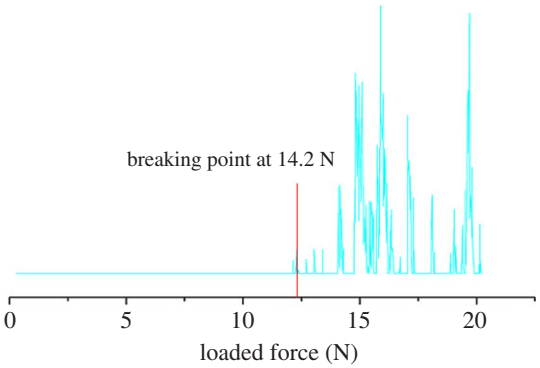

Figure 2. The typical scratch test results that illustrate adhesion between plasma SiO_x:H coatings (TMS:O_2 = 1:0) and the silicon wafer substrates, with a scanning range of 2 mm. The diameter of the diamond indenter was 0.2 mm, load speed was 20 N min^{-1}, and speed was 2 mm min^{-1}. The results obtained with all the plasma-coated samples ranged from 12.7 to 20.9 N.

1:0–1:5 were assessed and the adhesion forces of these plasma coatings ranged from 12.7 to 20.9 N (3.175×10^2 to 5.225×10^2 MPa). These results demonstrated that the plasma coatings were tightly integrated with the substrate, which could be applied in the surface modification of implanted biomaterials.

3.2. X-ray photoelectron spectra

Figure 3*a* shows the XPS survey spectra of SiO_x:H plasma nanocoatings in the binding energy range of 0–1200 eV. Only three elements', O1s, C1s and Si2p (Si2s peak is not discussed here because the atomic scattering factor is small) peaks could be found. Notably, the O element appeared in the plasma coatings obtained with TMS:O_2 = 1:0 (0 sccm O_2) owing to the post-reactions of the plasma coatings when exposed to ambient air.

Figure 3*b–d* shows the high-resolution spectra of Si2p, O1s and C1s electron orbital of SiO_x:H plasma nanocoatings prepared at different TMS/O_2 ratios (from 1:0 to 1:5 sccm). The Si2p peak could be deconvoluted into three peaks including SiO_2–C_2 (101.6 eV), SiO_3–C (102.7 eV) and Si–O_2 (103.7 eV), respectively [24]. It was noted that incorporation of Si–C (99.6 eV) and SiO–C_3 (100.5 eV) peaks would not give a good curve fitting with the Si2p spectra for all the samples. Calculation of the relative intensity of each peak using XPS peak 41 software showed that the component of SiO_2–C_2 decreased with the increase of O_2 flow ratio. These results indicate that more Si–CH_3 bonds of the TMS molecules were broken and replaced by Si–O bonds. As shown in figure 3, the O1s spectra exhibited three peaks at 531.65, 532.64 and 533.7 eV, which were attributed to C–OH, Si–O and O–Si–O bonds, respectively [25]. As seen in figure 3*d*, four peaks at 284 eV (Si–$(CH_3)_x$ bond), 284.85 eV (C–C bond), 285.6 eV (C–O bond) and 286.5 eV (C–OH bond) [26,27] were noticed with the plasma coatings prepared with TMS:O_2 ratios of 1:0 to 1:2. The Si–$(CH_3)_x$ peak (284 eV) could hardly be found for plasma coatings prepared with TMS:O_2 = 1:3. The results indicated that, with higher O_2 flow rate over 3 sccm (TMS = 1 sccm), the hydrophobic $-CH_3$ bonds in the TMS structure had all been almost detached and replaced by O-containing chemical groups. In addition, an amorphous SiO_x-like structure had been identified with these plasma coatings by X-ray diffraction in our previous study [8], and –OH, Si–O–Si and Si–H bonds were observed by Fourier-transform infrared spectroscopy [9].

Table 2 shows the percentage of each element (Si, C and O) of the plasma-deposited SiO_x:H nanocoatings by XPS quantification. It can be seen that, with the increase of O_2 flow rate or addition, the percentage of C component decreased, while the percentage of O component increased gradually. However, the percentage of Si component was constant in all six sample types with increase of O_2 flow rate.

3.3. Cell adhesion

Cells' attachment to plasma nanocoating surfaces was assessed by seeding EA.hy926 cells on the specimens (three specimens from each plasma coating) with a density of 1.0×10^3 cells ml^{-1}. Five examination areas were randomly chosen from each specimen for cell counting.

The attached cell numbers were statistically analysed and the results are shown in figure 4. With 4 h incubation, cells with different behaviours (suspension, just adhesion not spreading and spreading; figure 4*a*) could be easily distinguished. Statistical analyses showed no significant differences ($p > 0.05$) in numbers of cells adhering to all specimens at 4 h. However, after 8 h cell culture, most cells showed spreading behaviour, and the number of cells at the adhesion and suspension status decreased. The numbers of total and spreading cells adhered to 1:4 and 1:5 specimens were significantly higher than that on the 1:0 and 1:1 groups ($p < 0.05$). Cells adhered to surfaces would experience proliferation after 8 h culture, at the same time, more suspending cells would adhere to hydrophilic surfaces than to hydrophobic surfaces. It is demonstrated that hydrophilic SiO_x:H surfaces could promote higher cell adhesion and spreading when compared with hydrophobic surfaces.

Cell adhesion is closely coupled with the protrusions of the leading edge of the cell (filopodia and lamellipodia) [28]. The confocal immunofluorescence images of F-actin staining after 1 day of cell culture are shown in figure 5. It could be seen that there are obvious differences in single cell morphology observed among the cells attached to the SiO_x:H plasma nanocoated specimens. In 1:0 and 1:1 hydrophobic groups, all spreading cells showed polymerized F-actin filaments, more obvious protrusions (spike-like filopodias marked in red arrows and flat fan-like lamellipodias marked in white arrows in figure 5), those of which were in favour of cell migration. However, in 1:2–1:5 samples, filopodia and lamellipodia of cells were less than that of 1:0 and 1:1 samples. In addition, after 5 days of cell culture, the results of cell micromorphology by scanning electron microscopy (SEM) exhibited similar differences (shown in electronic supplementary material, figure S1), with cells attached on 1:0 and 1:1 hydrophobic surfaces

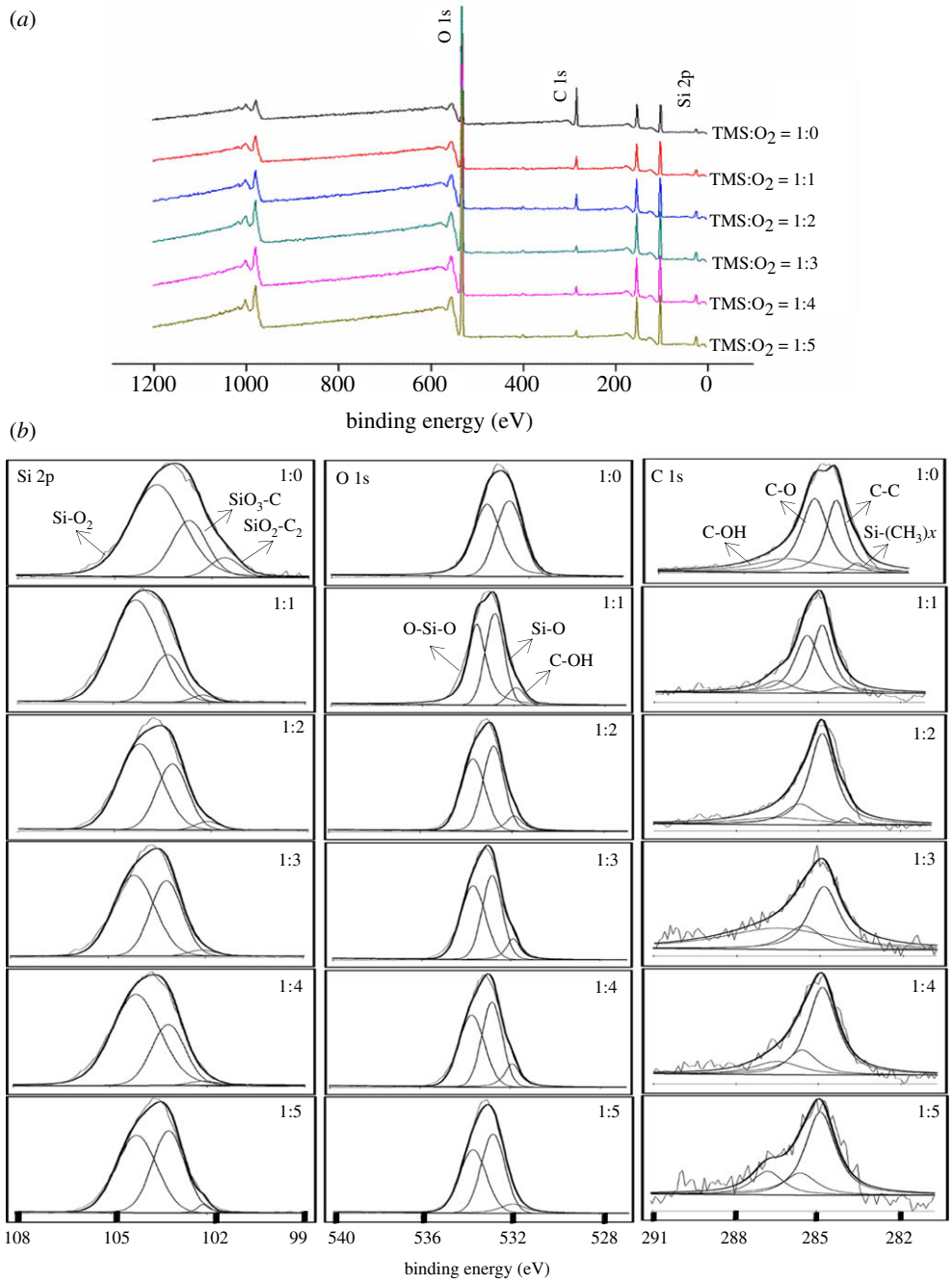

Figure 3. XPS spectra measured on the SiO_x:H plasma nanocoatings. (*a*) Full-scale survey spectra, (*b*) Si 2p electron orbital, (*c*) O 1s electron orbital, and (*d*) C 1s electron orbital.

Table 2. The percentage of each element in the SiO_x:H plasma nanocoatings by XPS quantification.

	TMS:O_2 ratio					
element (%)	1:0	1:1	1:2	1:3	1:4	1:5
Si	31.44	36.27	35.61	37.71	37.07	37.4
C	32.83	12.69	13.65	4.92	6.33	5.51
O	35.73	51.04	50.74	57.37	56.6	57.09

displaying obvious natural endothelial cobblestone road shape, while cells on 1:2–1:5 groups showed less filopodia and lamellipodia. The SEM results of 5 days' cell culture on plasma SiO_x:H surfaces with varying wettabilities confirmed the confocal immunofluorescence results of 1 day cell culture.

3.4. Cells' migration–scratch wound migration assay

The results of cells' migration by scratch wound migration assay are shown in figure 6. It can be seen from figure 6*b* that hydrophobic surfaces (1:0 and 1:1 groups, with contact angles $> 65^\circ$) showed the largest migration distance at almost every duration when compared with the other groups. Data analyses revealed that the cell migration distance on 1:0 and 1:1 samples was significantly longer than that on 1:5 samples at 2 h; the cell migration distance on 1:0 and 1:1 samples were

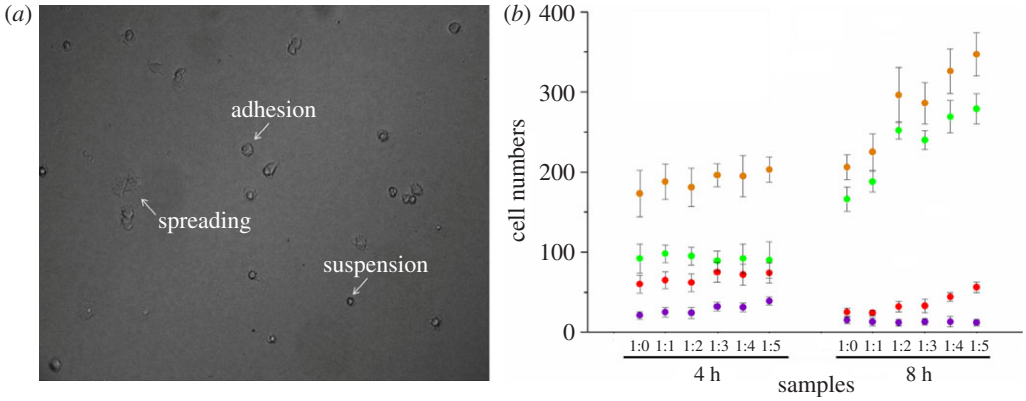

Figure 4. EA.hy926 cells adhered to SiO_x:H plasma nanocoating surfaces. (*a*) Representative image of the EA.hy926 cells adhered to SiO_x:H plasma nanocoating surfaces at different status (suspension, adhesion and spreading) after 4 h of culture. (*b*) Statistic analyses of the number of cells in suspension, adhesion and spreading status. Total cell numbers at 4 and 8 h were calculated and presented as mean ± s.d. Purple circles, suspension; red circles, adhesion; green circles, spreading; orange circles, total.

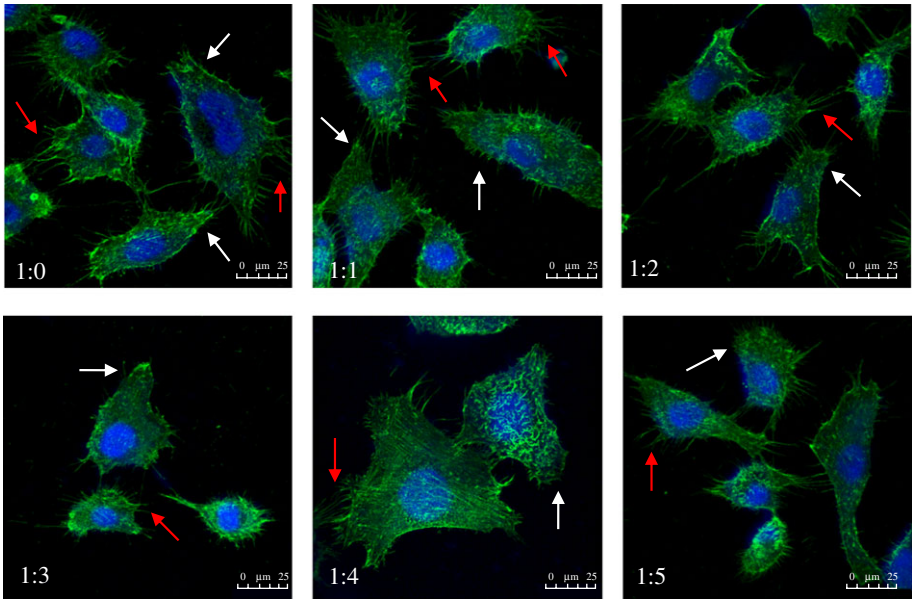

Figure 5. Confocal immunofluorescence images of EA.hy926 cells, showing localization of F-actin in response to the plasma SiO_x:H surfaces with varying wettabilities (green: F-actin; blue: nucleus). Red and white arrows in figures indicate filopodia and lamellipodia protrusion of cells, respectively.

significantly longer than that on 1:2 and 1:4 samples at 6 h; and the cell migration distance on 1:0 samples was significantly longer than that on the other groups at 12 h. The results of the average distance of migrated cells across the baseline (figure 6*c*) and wound repair duration (figure 6*d*) also demonstrated that the hydrophobic surfaces could enhance cell migration. Specifically, the wound repair duration (endothelialization in the scratch area) of 1:0 samples required about 18 h, shorter than that of 1:5 samples (about 24 h). The data of EC migration showed an obvious trend, i.e. that cells migrated faster on hydrophobic surfaces than on hydrophilic surfaces except 1:2 samples. Notably, the 1:2 samples (contact angles $\approx 50^\circ$) were abnormal among all samples. Migrated distance, the average migrated cells' number and wound repair duration data of 1:2 samples showed lower cell motility when compared with more hydrophilic samples (1:3 and 1:4 samples).

Interestingly, when compared with cell adhesion results shown in figure 4, cell migration results showed opposite trends to the cell adhesion behaviour on these plasma nanocoating surfaces. In other words, the hydrophilic surfaces could enhance cell adhesion, whereas the hydrophobic surfaces could promote cell migration. A possible explanation is that the stronger cell adhesion to hydrophilic surfaces is likely to keep cells attached to the surface, and thereby reduce their cell motility. These results are consistent with the reported regulation data of ECM such as LN and FN on cell migration [29].

3.5. Single cells' motility on wettable surfaces

According to images obtained at the start (0 min) and end points (30 min), the migrated distance of each single cell was calculated (figure 7*a*). The single cells migrating on surfaces with varying wettabilities showed

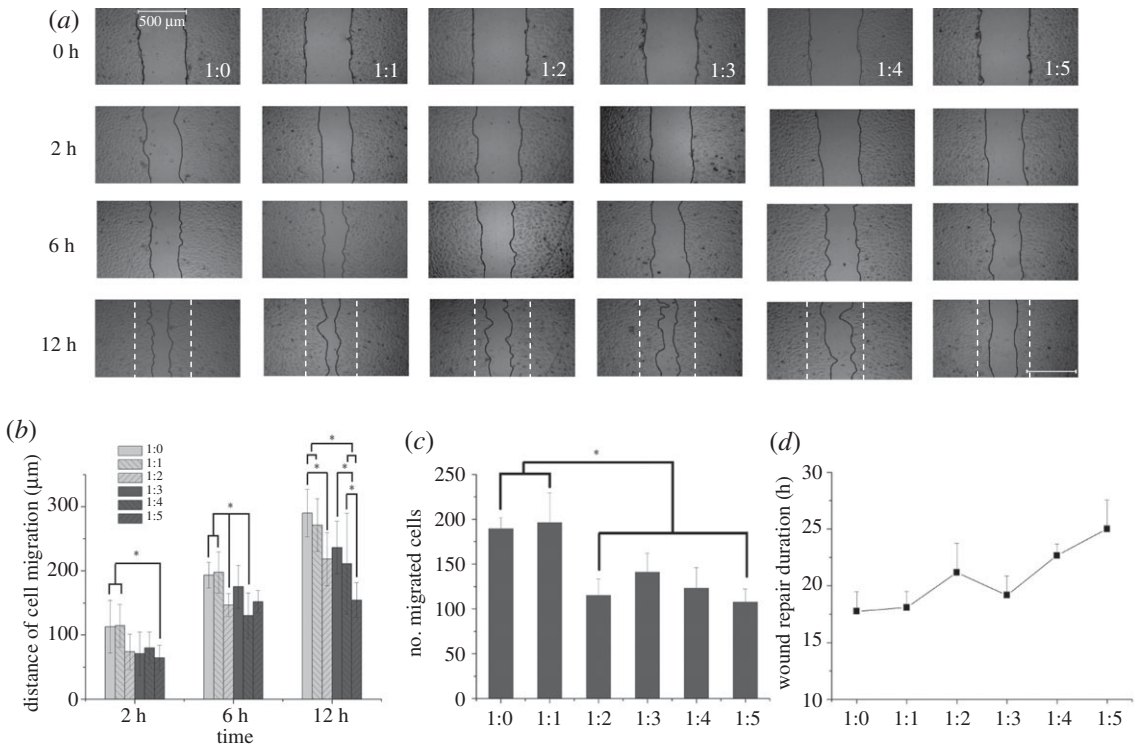

Figure 6. Effects of surface wettability on the migration of EA.hy926 cells. (*a*) Images illustrating cell migration on SiO_x:H plasma nanocoating surfaces at 0, 2, 6 and 12 h (scale bar, 500 μm). (*b*) Cell migration distance on the various surfaces tested. (*c*) Average number of migrated cells across the baseline (dashed line in (*a*)). (*d*) Wound repair duration on the plasma SiO_x:H coatings with different surface wettability. Asterisk denotes statistically significant difference with $p < 0.05$.

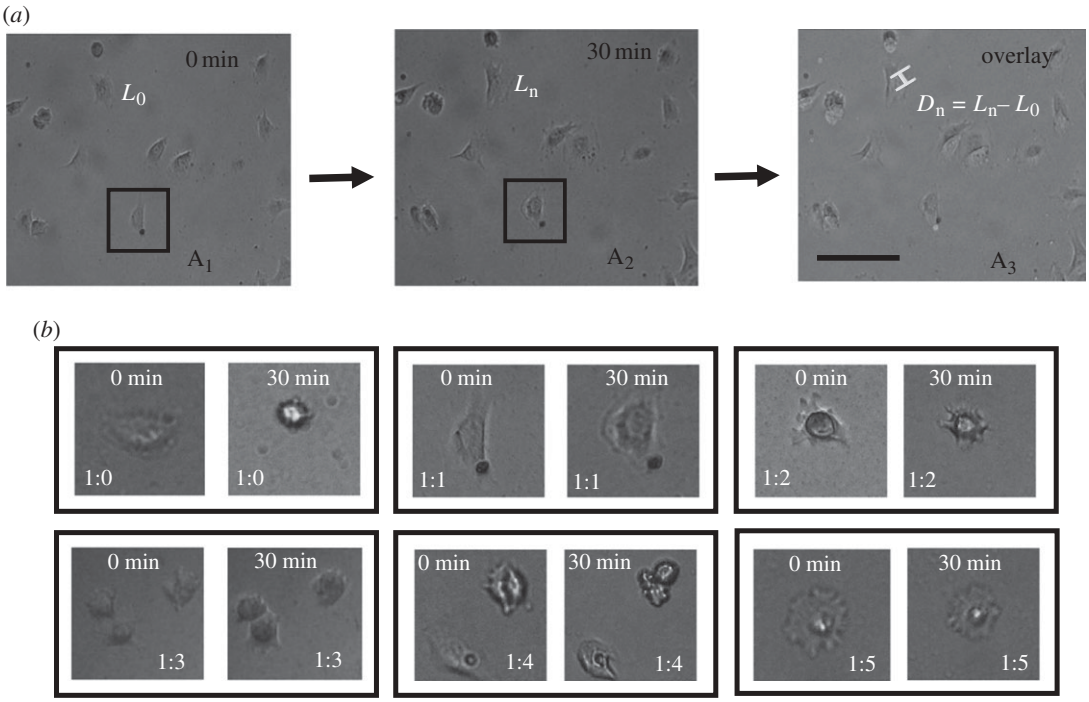

Figure 7. Effects of surface wettability on single EA.hy926 cells migration. (*a*) Images of single EA.hy926 cell migration on the plasma SiO_x:H surfaces: (A_1) initial location of cells at 0 min, (A_2) cell positioning at the ending point (30 min) and (A_3) overlay of the two previous images to show cells' motility on the surfaces tested. The distances migrated by single cells were calculated by $D_n = L_n - L_0$. The cell average migration speed on each group during 30 min was calculated accordingly and is shown in table 3 (only 1:1 sample group is shown in (*a*); the single cell in black pane in figures A_1 and A_2 was randomly selected and showed in (*b*) 1:1 group). (*b*) Morphological changes of single cells on the plasma SiO_x:H nanocoatings with different wettabilities. Scale bar, 100 μm.

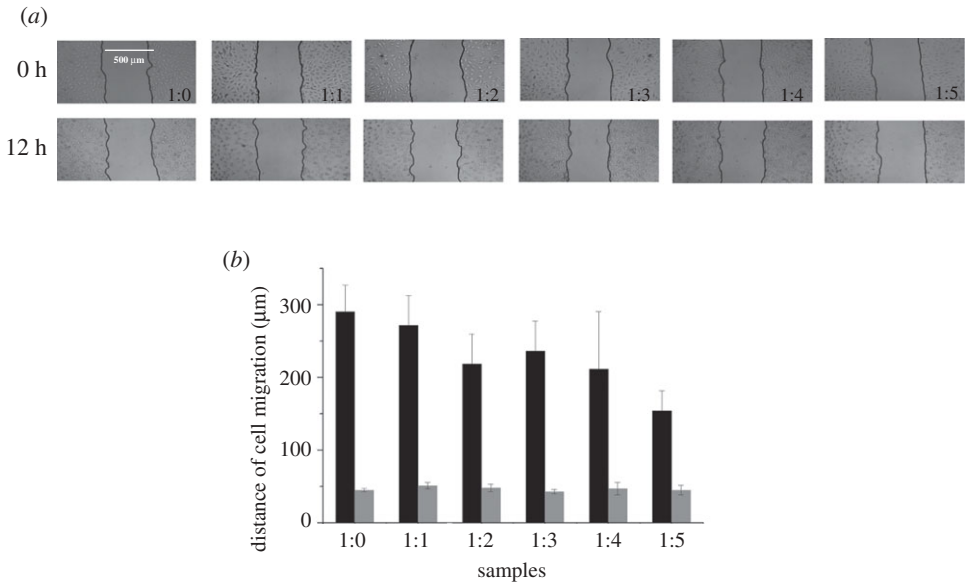

Figure 8. Effects of FAK inhibitor on the migration of single EA.hy926 cells on surfaces with different wettabilities at 0 and 12 h. The cells on each sample showed less migrated distance at 12 h. (Scale bar = 500 µm). (*a*) Images of cell migration on SiO_x:H plasma nanocoating surfaces at 0 and 12 h. (*b*) Cell migration distance with (grey bars) or without FAK addition (black bars).

Table 3. Single cells' migration on SiO_x:H plasma nanocoatings with different wettabilities.

	1:0	1:1	1:2	1:3	1:4	1:5
maximum migrated distance in 30 min (µm)	32.7	37.9	27.0	39.9	33.4	21.0
minimum migrated distance in 30 min (µm)	10.5	16.8	12.9	12.0	6.0	12.5
speed of single cells migration (µm min^{-1})	0.80 ± 0.23	0.87 ± 0.21	0.62 ± 0.13[a]	0.69 ± 0.31	0.59 ± 0.2[a]	0.60 ± 013[a]

[a]Means significant difference compared with 1:1 sample ($p < 0.05$).

different motilities. It can be seen from figure 7 and table 3 that 1:1 samples revealed the fastest migration speed during 30 min. Also, the cell migration speeds on the hydrophobic surfaces (1:0 and 1:1) were significantly faster than those on the hydrophilic surfaces (from 1:2 to 1:5 samples). However, maximum and minimum migrated distances of single cells in each group in 30 min showed no regularity owing to non-directional motion. The results also indicated that surface hydrophobicity had the advantage of surface hydrophilicity in enhancing cell migration speed.

3.6. Effect of FAK inhibitor on cell adhesion and migration

FAK inhibitor, 1, 2, 4, 5-benzenetetraamine tetrahydrochloride, would change in colour with duration as formation of large conjugated bonds between benzene and amino, and the chemical equation is depicted in electronic supplementary material, figure S2*a*. Therefore, freshly prepared FAK inhibitor was used in the whole study.

At first, the effects of different concentrations (from 50 to 250 nmol ml^{-1}) of FAK inhibitor on the adhesion of EA.hy926 cells cultured in TCPS at 4 h were examined (see electronic supplementary material, figure S2*b*). With the increase in the concentration of the FAK inhibitor, the cell nucleus became more apparent and the lamellipodia of spreading cells shrank. In particular with the addition of 200 and 250 nmol ml^{-1} FAK inhibitor, the lamellipodia of the cells almost disappeared. Therefore, the FAK inhibitor significantly increases cell detachment.

Different concentrations of FAK inhibitor could decrease EC migration in TCPS, which is shown in electronic supplementary material, figure S3*a*,*b*. It can be seen from electronic supplementary material, figure S3 that, with increasing concentrations of FAK inhibitor, the cell migration distance decreased. According to the results of electronic supplementary material, figure S3, 50 nmol ml^{-1} of FAK inhibitor were chosen to check if it could inhibit cell migration on plasma SiO_x:H coating (figure 8). The cell migration on different surfaces with different wettabilities decreased at 12 h, which was compared with previous results in figure 6 (without the addition of FAK inhibitor). In addition, there is no significant differences among all hydrophilic and hydrophobic groups. It is hypothesized that FAK played a central role in signalling, which was associated with EC migration on the surface of materials.

The behaviours of single cells were observed and characterized with 50 nmol ml^{-1} of FAK inhibitor treatment for 4 h. With the effect of FAK inhibitor for 4 h,

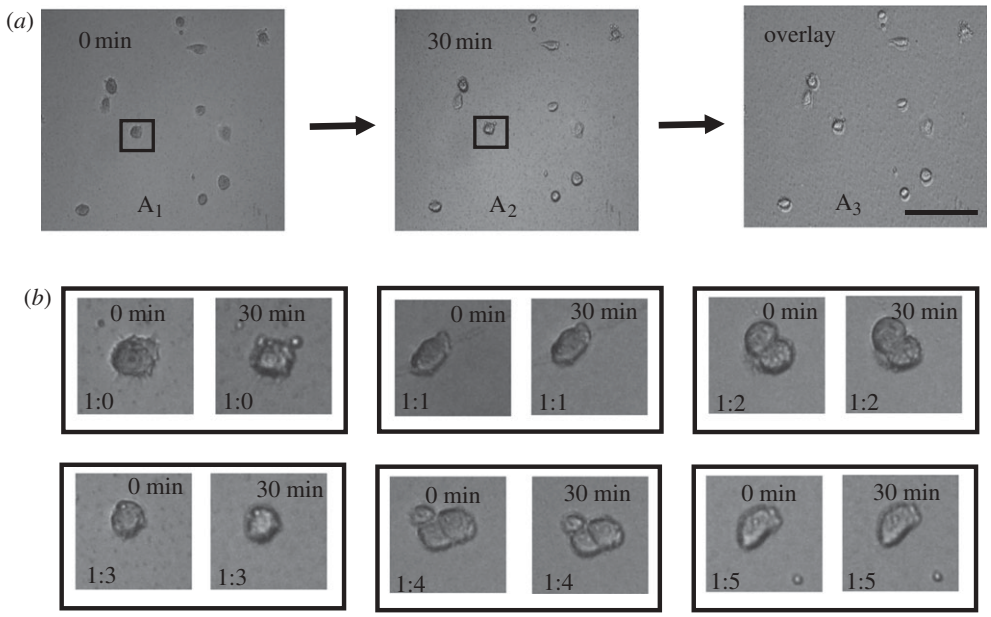

Figure 9. Effects of FAK inhititor on the migration of single EA.hy926 cells on surfaces with varying wettabilities. (*a*) Images of single EA.hy926 cells' migration on the plasma SiO_x:H surfaces with FAK inhibitor at 0 and 30 min (only 1:0 sample group is shown in (*a*); the single cell in black pane in figures A_1 and A_2 was randomly selected and showed in (*b*) 1:0 group). (A_1) Initial location of cells at 0 min, (A_2) cell positioning at the end point (30 min) and (A_3) overlay of the two previous images to show cells' motility on the surfaces tested. (*b*) Morphological changes of single cells on the plasma SiO_x:H nanocoatings with different wettabilities, using 50 nmol ml^{-1} FAK inhibitor. The single cells on each sample showed no obvious changes in morphology or distance migrated in 30 min duration. Scale bar, 100 μm.

most cells on surfaces with different wettabilities showed round morphology and no obvious changes in the subsequent 30 min observation (figure 9*b*). Furthermore, migrated distance was hardly found among these cells during 30 min (figure 9*a*). It is noted that FAK inhibitor could significantly restrain cell motility on the different surface wettabilities.

3.7. Associated protein expression in FAK-Rho GTPases signalling pathway

Cell migration-dependent FAK-Rho GTPases signalling pathway has been proven in a previous study [17]. However, does EC migration behaviour on surfaces with different wettabilities follow this signalling event? Expression of some crucial proteins in the FAK-Rho GTPases signalling pathway by Western blot and immunofluorescence is shown in figure 10.

It can be seen from figure 10*a–c* that proteins in the FAK-Rho GTPases signalling pathway, in response to plasma SiO_x:H surfaces with varying wettabilities, showed significant differences. It is demonstrated that the surface wettability could lead to the expression of different proteins, and resulted in diverse cell adhesion and migration behaviours. The integrin subunits, $\alpha 5$ and $\alpha 2$, which are respective receptors of FN and LN, showed opposite expression levels in response to plasma SiO_x:H surfaces (figure 10*a*). Hydrophobic surfaces (1:0 and 1:1 groups) and most hydrophilic surfaces (1:5 group) revealed higher integrin $\alpha 5$ but lower integrin $\alpha 2$ expression, suggesting that plasma SiO_x:H nanocoatings with different wettabilities could adsorb different ECM proteins and result in differences in integrin expression. Regarding the FAK and *p*-FAK proteins, it could be seen from figure 10*b* that the total FAK proteins in all samples were approximately equal. However, the phosphorylation level of FAK (*p*-FAK) was downregulated with increasing surface wettability. The small G protein RhoA (figure 10*c*), which regulates stress fibres related to cell adhesion/migration, showed equal expression levels in 1:0–1:4 samples, but a relatively lower level in 1:5 groups. Another small G protein, Rac1, which regulates lamellipodia, exhibited an interesting phenomenon. The hydrophobic surfaces (1:0 group) showed higher expression level of Rac1 than that of hydrophilic surfaces (1:2–1:5 groups). Among 1:2–1:5 groups, 1:2 and 1:5 samples showed lowest Rac1 expression, which was consistent with previous results of cell migration (figure 6). The immunofluorescence results in figure 10*d*,*e* revealed that Rac1 was mainly distributed in the cytoplasm, while RhoA was distributed both in the cytoplasm and the nucleus. In addition, it verified the Western blot results in which cells on 1:2 and 1:5 samples showed weaker expression of Rac1 protein (figure 10*e*), and only 1:5 group showed lower expression of RhoA protein (figure 10*d*).

Specially, compared with more hydrophilic samples (1:3 and 1:4 samples), 1:2 samples showed a lower integrin $\alpha 5$ and Rac1 expression level. Meanwhile, the *p*-FAK expression of 1:2 samples presented a threshold. Based on previous results of cell migration (figure 6), 1:2 samples also showed lower cell motility. We speculated that 1:2 samples were a key turning point, i.e. cell adhesion/migration on hydrophobic surfaces (1:0 and 1:1) involved the FAK-Rho GTPases signalling pathway, while on hydrophilic surfaces (1:2–1:5

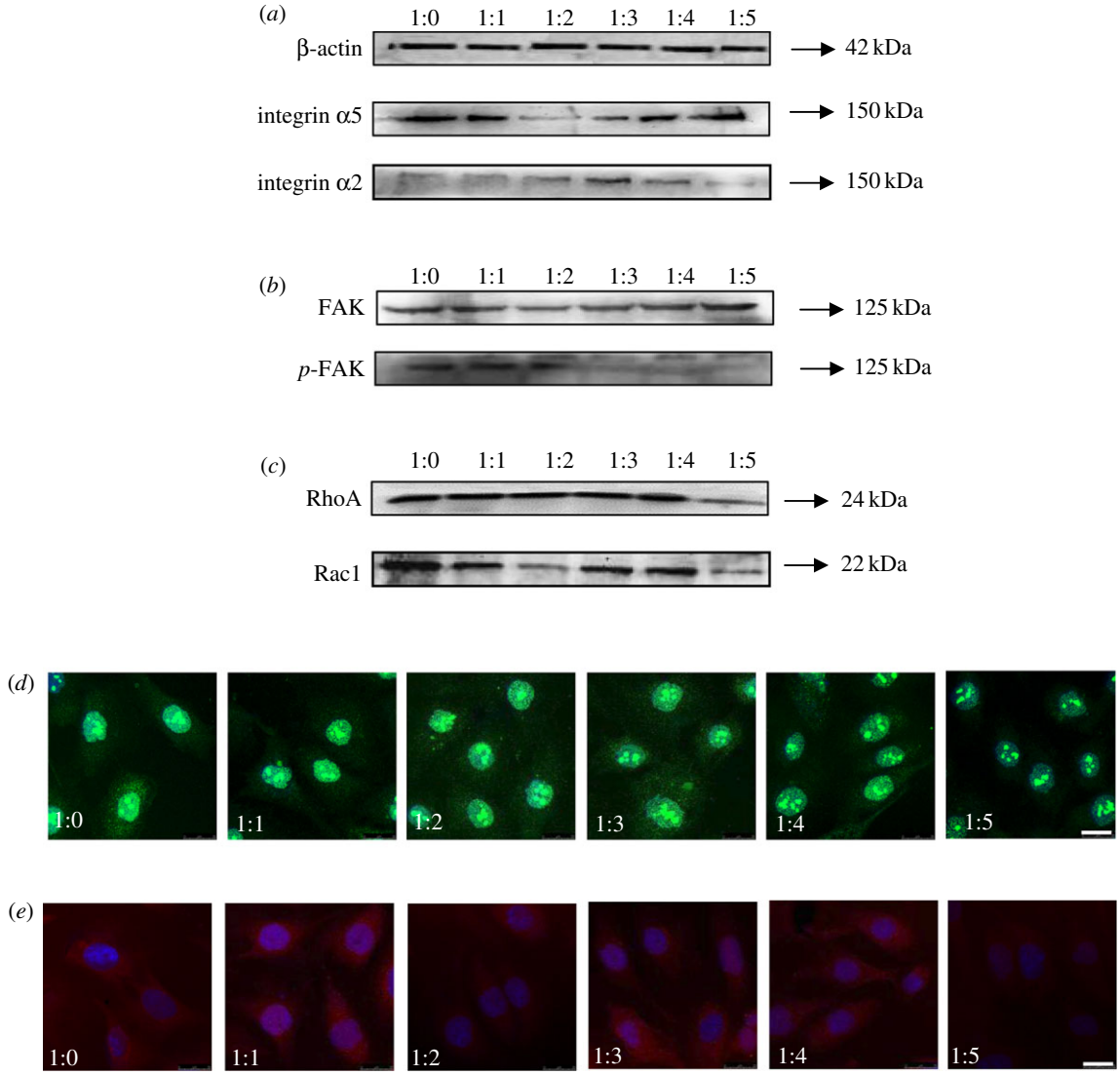

Figure 10. Western blot analyses of the effects of plasma SiO_x:H surfaces with varying wettabilities on: (*a*) cell membrane receptors—integrins' $\alpha 2$ and $\alpha 5$ protein expression; (*b*) FAK and *p*-FAK protein expression; (*c*) small G protein—RhoA and Rac1 protein expression. Immunofluorescence analyses of the effects of SiO_x:H surfaces on protein distribution and expression of: (*d*) RhoA (green) and (*e*) Rac1 (red) (blue: nucleus). (*d*,*e*) Scale bar, 25 μm.

groups, with contact angles from $47.5 \pm 3.0^\circ$ to $26.3 \pm 4.0^\circ$), the signalling events of cell adhesion/migration were uncertain to the FAK-Rho GTPases pathway. Notably, 1:5 samples showed significantly less migration distance at 12 h (figure 6), and lower RhoA and Rac1 protein expression levels compared with 1:4 samples, while the difference in contact angle was only about 3° ($29.3 \pm 2.5^\circ$ versus $26.3 \pm 4.0^\circ$). In addition, according to the results in figure 8, the FAK inhibitor could decrease cell migrated distance in all samples, suggesting that FAK phosphorylation at the 397 tyrosine site was an important event for EC migration. Two critical proteins relevant to cell migration, *p*-FAK and Rac1, both showed stronger expression levels in hydrophobic surfaces than in hydrophilic surfaces. This is in agreement with results showing that hydrophobic surfaces could promote migration of ECs. As a result, it is also certified that the FAK-Rho GTPases signalling pathways can be correlated to EC migration on hydrophobic plasma SiO_x:H surfaces. The 1:2 samples revealed higher levels of *p*FAK but lower levels of Rac1, the 1:3 and 1:4 samples showed lower levels of *p*FAK but higher levels of Rac1, while the 1:5 samples showed lower levels of *p*FAK, Rac1 and RhoA. Therefore, cells migrating in the 1:2–1:5 groups probably experienced other different signalling pathways. For example, FAK–PI3K (the phosphoinositide 3-kinases) was mentioned in an alternative work [30]. In light of previous FAK inhibitor results, EC migration on both hydrophobic and hydrophilic plasma SiO_x:H coatings was FAK (pY^{397})-dependent, but as to 1:2–1:5 groups, cell migration on coatings was uncertain to the FAK-Rho GTPases signalling pathways.

4. DISCUSSION

Using plasma-associated technology such as plasma immersion ion implantation deposition (PIII) and plasma-enhanced chemical vapour deposition (PECVD),

Ti–O, T–Ni and amorphous carbon (a-C:H) films were prepared and exhibited excellent biocompatibility [31–33]. Plasma-nanocoated SiO_x:H films showed stable chemical and mechanical properties. Even after repeatedly using samples (experiencing cleaning and collecting deposited proteins using a plastic cell scrapper), the contact angles have hardly changed. It suggested that plasma-nanocoated SiO_x:H films could be applied for the surface modification of implanted materials because of its well-controllable and stable properties. In preliminary studies in our research group, this coating (only $TMS:O_2 = 1:4$ condition) has been used to modify intravascular stents and implanted in the rabbit abdominal artery. The preliminary results showed that plasma-nanocoated SiO_x:H films could accelerate re-endothelialization and inhibit restenosis (data not shown). Certainly, more animals should be used in our further research in order to collect statistically reliable data.

In this study, EA.hy926 cells instead of original ECs were used because of their higher affinity to the surfaces of materials. Actually, the primary HUVECs purchased from Sciencell were tested as a model cell type in our entire experiments. However, we found that HUVECs showed low affinity to surfaces without FN or collagen pre-coatings. In most available published similar works [12,34,35], surfaces are coated with different FN concentrations and blocked by serum albumin. The EA.hy926 cells, which retain most features of HUVECs, showed better adhesion capacity *in vitro* and made contact with the plasma SiO_x:H nanocoating directly without FN introduction.

The surface properties of an implant, especially surface wettability and chemistry, play a critical role in determining its biocompatibility and ultimately its integration into the natural biological system of a human body, as soon as it directly contacts the blood and host tissues. Recently, self-assembled monolayers were regarded as a conventional model substrate for mechanistic investigation of adhesion of cells and platelets [36]. Ordered and well-controlled surface functional groups ($-CH_3$, $-COOH$, $-OH$ and $-NH_2$) grafted on SAMs induced changes of wettability and were used to study cell adhesion behaviour and correlate it with the FAK signalling pathway [34], and adsorption and activation of plasma proteins (fibrinogen and albumin) [37]. According to these studies [38], the surfaces prepared with different concentrations (100/0, 34/66, 50/50, 83/17, 0/100) of two kinds of thiol ($HS–(CH_2)_{10}–CH_3$ and $HS–(CH_2)_{10}–COOH$) had contact angles from $111 \pm 3.5^\circ$ to $21 \pm 7.1^\circ$, which were in a similar range to that of the SiO_x:H plasma nanocoating surfaces used in the present study. The literature results showed that the number of adhered HUVECs reached a maximum on CH_3/OH-mixed SAMs with a water contact angle of 40°, while cell adhesion decreased with increasing water contact angle up to $60–70^\circ$, suggesting that cell adhesion is mainly determined by surface wettability, but is also affected by the surface functional groups, their surface density and the cell type [13]. Our results showed that cell adhesion reached a maximum on hydrophilic 1:4 samples (with contact angle of $29.3 \pm 2.5^\circ$) and on 1:5 samples (with contact angle of $26.3 \pm 4.0^\circ$) after 8 h of cell culture.

Cell migration is an essential process in angiogenesis, wound healing, vessel remodelling and re-endothelialization, which involves formation, remodelling and disassembly of focal adhesion. It can be divided into four distinct steps: (i) lamellipodia formation at the cell periphery without directional preference; (ii) directional lamellipodia protrusion and new focal adhesion formation in the flow direction; (iii) remodelling of pre-existing focal adhesions; and (iv) disassembly of focal adhesions at the rear [39]. As early as 1991, Calof & Lander [29] demonstrated the relationship between neuronal cell migration and cell–substratum adhesion and reported that LN promoted neuronal migration, but was anti-adhesion. Similarly, our results shown in figures 4 and 6 demonstrate that cell adhesion and cell migration behaviours occur in very different ways, and are probably affected by adhesion strength between cells and the substrate. Strong adhesion between cells and substrate could enhance cell attachment but inhibit the cell migration. Van Kooten *et al.* [40] reported that cell detachment decreased with increasing wettability. They suggested that cells adhered to hydrophilic surfaces presented stronger adhesion strength than those adhered to hydrophobic surfaces, resulting in improved cell adhesion. However, strong adhesion is likely to keep cells attached on the surface, and thereby preventing cell migration. To our knowledge, there are only a few reported works about EC migration on surfaces with varying wettabilities. In the present study, results show that hydrophilic surfaces can enhance EC adhesion, but hydrophobic surfaces can greatly accelerate EC migration. To date, most investigations on biomaterials usually focus on cell adhesion and not cell migration [14,41,42]. As a continuation of this study, we are currently investigating surface wettability effects on cell migration under gradient laminar shear stress, with the aim of establishing a relationship between surface wettability and cell adhesion, adhesion force and cell migration.

In this study, FAK inhibitor was used to determine if (p)FAK was involved in cell adhesion and migration. We have demonstrated that hydrophilic surfaces could promote endothelial adhesion, but were anti-migration, thus showing that cell adhesion strength could play an important role in adhesion/migration. However, it remained unclear why the FAK inhibitor decreased both cell adhesion and migration behaviour. We speculated that dephosphorylation of FAK at the Y-397 site could interrupt downstream signalling events. The family of Rho-GTPases, RhoA, Rac and Cdc42, which participates in directing actin assembly into stress fibres, lamellipodia and filopodia, could be restrained by FAK inhibitor. The disassembly of stress fibres, lamellipodia and filopodia would increase cell detachment and reduce cell adhesion. At the same time, the absence of RhoA, Rac and Cdc42 could result in the decline of cell migration. Therefore, phosphorylation of FAK at the Y-397 site could be an important event in cell adhesion/migration on surfaces with distinct wettabilities.

Using SAMs as model substrates and MC3T3-E1 osteoblast-like cells, Kaselowsky *et al.* [15] performed a series of studies to demonstrate that surface chemistry

modulated FN adsorption following the pattern $NH_2 > CH_3 > COOH > OH$, and $\alpha5\beta1$ integrin binding following the order $OH > COOH = NH_2 > CH_3$. They also found that surface chemistry induced FAK phosphorylation at, respectively, 576, 397 and 861 tyrosine sites following the order $NH_2 > OH = COOH > CH_3$ [34]. However, several differences can be pointed out with our results. The possible reason is that gene and protein expression of cells are affected not only by wettability but also by surface chemistry and composition. In addition, the cell type and culture duration are also crucial factors. In this study, the expressions of related proteins in the FAK-Rho GTPases signalling pathways were examined. Based on results of cell migration, FAK inhibition and protein expression, we demonstrated that EC migration on all hydrophobic or hydrophilic plasma SiO_x:H surfaces would depend on the phosphorylation of FAK at the 397 sites, and EC migration on hydrophobic surfaces involved the FAK-Rho GTPases signalling pathways. We also speculated that there are other signalling pathways involved in EC migration on hydrophilic plasma SiO_x:H surfaces, which also depend on FAK phosphorylation but are uncertain to depend on Rho GTPases. Cell behaviour on 1:2 sample is a turning point.

Some signalling pathways or signalling molecules involved in cell migration were already identified [43]. For example, the association between EC migration on polyurethane nanocomposites and VEGFR2-PI3K-Akt-eNos-NO signalling pathways has been demonstrated by Hung *et al.* [30], who further suspected that FAK-Rho GTPases were another signalling event involved in cell migration. In the present study, we confirmed that EC migration behaviour on hydrophobic plasma SiO_x:H surfaces can be correlated with the FAK-Rho GTPases signalling events, and the FAK phosphorylation at Y^{397} was a key factor for EC migration on all samples. However, cell adhesion and migration processes are dynamic and persistent behaviours. Protein expression would alter with an increase in cell–substrate contact duration. In this study, considering that enough concentrations were used for Western blot analyses, we collected cells at 48 h at 70–80% confluence. Despite the encouraging results obtained, several new questions were raised, such as: how do cells sense surface wettability and protein expressions at the initial stages? Do proteins in the FAK-Rho GTPases change at a certain proportion with cell contact duration? These questions will be explored in our future research.

5. CONCLUSION

In this study, significant new information is presented: (i) biocompatible plasma SiO_x:H nanocoatings were prepared with well-controllable surface wettability and showing strong adhesion force with the substrate. This technology may be applied for the surface modification of implantable biomaterials, such as coronary stents. (ii) EC adhesion and migration showed opposite behaviours on the hydrophilic/hydrophobic surfaces of plasma SiO_x:H nanocoatings. Hydrophobic surfaces could promote higher EC migration than hydrophilic surfaces. The number of adherent ECs showed a maximum on hydrophilic surfaces, while cells adhered to hydrophobic surfaces exhibited a tendency for cell migration. (iii) EC migration on hydrophilic/hydrophobic surfaces of plasma SiO_x:H nanocoatings involved differences in the expression of multiple proteins, including integrins, (*p*)FAK, Rac1 and RhoA in the FAK-Rho GTPases signalling event. The FAK-Rho GTPases signalling pathway was correlated with EC migration on hydrophobic plasma SiO_x:H surfaces.

This study was partly supported by National Natural Science Foundation of China (30970721 and 10772127), Chinese Postdoctoral Science Foundation (20090461340 and 201003702) and China Medical Board (82-412). The authors are grateful to Prof. Xiaojing Liu, Mr Jianjun Hu and Mr Juhui Qiu for their helpful discussions and assistance in this study.

REFERENCES

1 Lamalice, L., Le Boeuf, F. & Huot, J. 2007 Endothelial cell migration during angiogenesis. *Circ. Res. Mar.* **6**, 782–794. (doi:10.1161/01.RES.0000259593.07661.1e)

2 Jakabcin, J., Bystron, M., Spacek, R., Veselka, J., Kvasnak, M., Kala, P., Maly, J. & Cervinka, P. 2008 The lack of endothelization after drug-eluting stent implantation as a cause of fatal late stent thrombosis. *J. Thromb. Thrombolysis* **2**, 154–158. (doi:10.1007/s11239-007-0080-2)

3 Palmaz, J. C., Benson, A. & Sprague, E. A. 1999 Influence of surface topography on endothelialization of intravascular metallic material. *J. Vasc. Interv. Radiol.* **4**, 439–444. (doi:10.1016/S1051-0443(99)70063-1)

4 Zampetaki, A., Kirton, J. P. & Xu, Q. 2008 Vascular repair by endothelial progenitor cells. *Cardiovasc. Res.* **78**, 413–421. (doi:10.1093/cvr/cvn081)

5 Lev, E. I. *et al.* 2010 Circulating endothelial progenitor cell levels and function in patients who experienced late coronary stent thrombosis. *Eur. Heart J.* **31**, 2625–2632. (doi:10.1093/eurheartj/ehq184)

6 Choukourov, A., Pihosh, Y., Stelmashuk, V., Biederman, H., Slavinska, D., Kormunda, M. & Zajickova, L. 2002 Rf sputtering of composite SiO_x/plasma polymer films and their basic properties. *Surf. Coat. Technol.* **151**, 214–217. (doi:10.1016/S0257-8972(01)01622-X)

7 Umezu, I., Yoshida, K., Sugimura, A., Inokuma, T., Hasegawa, S., Wakayama, Y., Yamada, Y. & Yoshida, T. 2000 A comparative study of the photoluminescence properties of a-SiO_x:H film and silicon nanocrystallites. *J. Non-Cryst. Solids.* **266**, 1029–1032. (doi:10.1016/S0022-3093(99)00896-0)

8 Wang, G., Shen, Y., Cao, Y., Yu, Q. & Guidoin, R. 2007 Biocompatibility study of plasma-coated nitinol (NiTi alloy) stents. *IET Nanobiotechnol.* **6**, 102–106. (doi:10.1049/iet-nbt:20070011)

9 Shen, Y., Wang, G., Chen, L., Li, H., Yu, P., Bai, M., Zhang, Q., Lee, J. & Yu, Q. 2009 Investigation of surface endothelialization on biomedical nitinol (NiTi) alloy: effects of surface micropatterning combined with plasma nanocoatings. *Acta Biomater.* **9**, 3593–3604. (doi:10.1016/j.actbio.2009.05.021)

10 Dahmen, C., Janotta, A., Dimova-Malinovska, D., Marx, S., Jeschke, B., Nies, B., Kessler, H. & Stutzmann, M. 2003 Surface functionalization of amorphous silicon

and silicon suboxides for biological applications. *Thin Solid Films* **1–2**, 201–207. (doi:10.1016/S0040-6090(02)01228-2)
11 Anselme, K. & Bigerelle, M. 2006 Modelling approach in cell/material interactions studies. *Biomaterials* **8**, 1187–1199. (doi:10.1016/j.biomaterials.2005.10.009)
12 Tzoneva, R., Faucheux, N. & Groth, T. 2007 Wettability of substrata controls cell–substrate and cell–cell adhesions. *Biochim. Biophys. Acta* **11**, 1538–1547.
13 Arima, Y. & Iwata, H. 2007 Effect of wettability and surface functional groups on protein adsorption and cell adhesion using well-defined mixed self-assembled monolayers. *Biomaterials* **20**, 3074–3082. (doi:10.1016/j.biomaterials.2007.03.013)
14 Barrias, C. C., Martins, M. C. L., Almeida-Porada, G., Barbosa, M. A. & Granja, P. L. 2009 The correlation between the adsorption of adhesive proteins and cell behaviour on hydroxyl-methyl mixed self-assembled monolayers. *Biomaterials* **3**, 307–316. (doi:10.1016/j.biomaterials.2008.09.048)
15 Keselowsky, B. G., Collard, D. M. & Garcia, A. J. 2003 Surface chemistry modulates fibronectin conformation and directs integrin binding and specificity to control cell adhesion. *J. Biomed. Mater. Res. A* **2**, 247–259. (doi:10.1002/jbm.a.10537)
16 Belkin, A. M. & Stepp, M. A. 2000 Integrins as receptors for laminins. *Microsc. Res. Technique* **3**, 280–301. (doi:10.1002/1097-0029(20001101)51:3<280::AID-JEMT7>3.0.CO;2-O)
17 Mitra, S. K., Hanson, D. A. & Schlaepfer, D. D. 2005 Focal adhesion kinase: in command and control of cell motility. *Nat. Rev. Mol. Cell. Biol.* **1**, 56–68. (doi:10.1038/nrm1549)
18 Raftopoulou, M. & Hall, A. 2004 Cell migration: Rho GTPases lead the way. *Dev. Biol.* **1**, 23–32. (doi:10.1016/j.ydbio.2003.06.003)
19 Bouis, D., Hospers, G. A., Meijer, C., Molema, G. & Mulder, N. H. 2001 Endothelium *in vitro*: a review of human vascular endothelial cell lines for blood vessel-related research. *Angiogenesis* **2**, 91–102. (doi:10.1023/A:1012259529167)
20 Tang, C. J., Wang, G. X., Shen, Y., Wan, L. J., Xiao, L., Zhang, Q., Yu, Q. S., Liu, L. S. & Wen, G. B. 2010 A study on surface endothelialization of plasma coated intravascular stents. *Surf. Coat. Technol.* **9–10**, 1487–1492. (doi:10.1016/j.surfcoat.2009.09.084)
21 Hsu, P. P., Li, S., Li, Y. S., Usami, S., Ratcliffe, A., Wang, X. & Chien, S. 2001 Effects of flow patterns on endothelial cell migration into a zone of mechanical denudation. *Biochem. Biophys. Res. Commun.* **3**, 751–759. (doi:10.1006/bbrc.2001.5221)
22 Golubovskaya, V. M., Nyberg, C., Zheng, M., Kweh, F., Magis, A., Ostrov, D. & Cance, W. G. 2008 A small molecule inhibitor, 1,2,4,5-benzenetetraamine tetrahydrochloride, targeting the y397 site of focal adhesion kinase decreases tumor growth. *J. Med. Chem.* **23**, 7405–7416. (doi:10.1021/jm800483v)
23 Vogler, E. A. 1998 Structure and reactivity of water at biomaterial surfaces. *Adv. Colloid Interface* **74**, 69–117. (doi:10.1016/S0001-8686(97)00040-7)
24 Heo, J., Kim, H. J., Han, J. & Shon, J. W. 2007 The structures of low dielectric constant SiOC thin films prepared by direct and remote plasma enhanced chemical vapor deposition. *Thin Solid Films* **12**, 5035–5039. (doi:10.1016/j.tsf.2006.10.095)
25 Li, H. X., Xu, T., Wang, C. B., Chen, J. M., Zhou, H. D. & Liu, H. W. 2006 Humidity dependence on the friction and wear behavior of diamond-like carbon film in air and nitrogen environments. *Diam. Relat. Mater.* **10**, 1585–1592. (doi:10.1016/j.diamond.2005.12.048)
26 Majumdar, A., Das, G., Patel, N., Mishra, P., Ghose, D. & Hippler, R. 2008 Microstructural and chemical evolution of -CH3-incorporated (Low-k) SiCO(H) films prepared by dielectric barrier discharge plasma. *J. Electrochem. Soc.* **1**, D22–D26. (doi:10.1149/1.2801345)
27 Jung, A. S., Navamathavan, R., Lee, K. M. & Choi, C. K. 2008 Plasma characteristics of low-k SiOC(-H) films prepared by using plasma enhanced chemical vapor deposition from DMDMS/O-2 precursors. *Surf. Coat. Technol.* **22–23**, 5693–5696. (doi:10.1016/j.surfcoat.2008.06.045)
28 Parsons, J. T., Horwitz, A. R. & Schwartz, M. A. 2010 Cell adhesion: integrating cytoskeletal dynamics and cellular tension. *Nat. Rev. Mol. Cell Biol.* **9**, 633–643. (doi:10.1038/nrm2957)
29 Calof, A. L. & Lander, A. D. 1991 Relationship between neuronal migration and cell-substratum adhesion: laminin and merosin promote olfactory neuronal migration but are anti-adhesive. *J. Cell. Biol.* **3**, 779–794. (doi:10.1083/jcb.115.3.779)
30 Hung, H. S., Wu, C. C., Chien, S. & Hsu, S. H. 2009 The behavior of endothelial cells on polyurethane nanocomposites and the associated signaling pathways. *Biomaterials* **8**, 1502–1511. (doi:10.1016/j.biomaterials.2008.12.003)
31 Yang, P., Kwok, S. C. H., Chu, P. K., Leng, Y. X., Chen, J. Y., Wang, J. & Huang, N. 2003 Haemocompatibility of hydrogenated amorphous carbon (a-C:H) films synthesized by plasma immersion ion implantation-deposition. *Nucl. Instrum. Methods B* **206**, 721–725. (doi:10.1016/S0168-583X(03)00871-1)
32 Yang, P., Huang, N., Leng, Y. X., Chen, J. Y., Sun, H., Wang, J. & Wan, G. J. 2004 Inhibition of adherent platelet activation produced by Ti-O thin film fabricated by PIII. *Surf. Coat. Technol.* **1–2**, 265–269. (doi:10.1016/j.surfcoat.2004.03.031)
33 Huang, N., Leng, Y. X., Yang, P., Chen, J. Y., Sun, H., Wang, J., Wan, G. J., Zhao, A. S. & Ding, P. D. 2006 Surface modification of coronary artery stent by Ti-O/Ti-N complex film coating prepared with plasma immersion ion implantation and deposition. *Nucl. Instrum. Methods B* **1–2**, 18–21. (doi:10.1016/j.nimb.2005.08.080)
34 Keselowsky, B. G., Collard, D. M. & Garcia, A. J. 2004 Surface chemistry modulates focal adhesion composition and signaling through changes in integrin binding. *Biomaterials* **28**, 5947–5954. (doi:10.1016/j.biomaterials.2004.01.062)
35 Lan, M. A., Gersbach, C. A., Michael, K. E., Keselowsky, B. G. & Garcia, A. J. 2005 Myoblast proliferation and differentiation on fibronectin-coated self-assembled monolayers presenting different surface chemistries. *Biomaterials* **22**, 4523–4531. (doi:10.1016/j.biomaterials.2004.11.028)
36 Faucheux, N., Schweiss, R., Lutzow, K., Werner, C. & Groth, T. 2004 Self-assembled monolayers with different terminating groups as model substrates for cell adhesion studies. *Biomaterials* **14**, 2721–2730. (doi:10.1016/j.biomaterials.2003.09.069)
37 Sivaraman, B. & Latour, R. A. 2010 The relationship between platelet adhesion on surfaces and the structure versus the amount of adsorbed fibrinogen. *Biomaterials* **5**, 832–839. (doi:10.1016/j.biomaterials.2009.10.008)
38 Sperling, C., Fischer, M., Maitz, M. F. & Werner, C. 2009 Blood coagulation on biomaterials requires the combination of distinct activation processes. *Biomaterials* **27**, 4447–4456. (doi:10.1016/j.biomaterials.2009.05.044)

39 Li, S., Huang, N. F. & Hsu, S. 2005 Mechanotransduction in endothelial cell migration. *J. Cell. Biochem.* **6**, 1110–1126. (doi:10.1002/jcb.20614)
40 van Kooten, T. G., Schakenraad, J. M., van der Mei, H. C. & Busscher, H. J. 1992 Influence of substratum wettability on the strength of adhesion of human fibroblasts. *Biomaterials* **13**, 897–904. (doi:10.1016/0142-9612(92)90112-2)
41 Pareta, R. A., Reising, A. B., Miller, T., Storey, D. & Webster, T. J. 2009 Increased endothelial cell adhesion on plasma modified nanostructured polymeric and metallic surfaces for vascular stent applications. *Biotechnol. Bioeng.* **3**, 459–471. (doi:10.1002/bit.22276)
42 Lu, J., Rao, M. P., MacDonald, N. C., Khang, D. & Webster, T. J. 2008 Improved endothelial cell adhesion and proliferation on patterned titanium surfaces with rationally designed, micrometer to nanometer features. *Acta Biomater.* **1**, 192–201. (doi:10.1016/j.actbio.2007.07.008)
43 Vicente-Manzanares, M., Webb, D. J. & Horwitz, A. R. 2005 Cell migration at a glance. *J. Cell Sci.* **21**, 3203–3208.